Improving Frequency Stability for Renewable Energy Power Plants with Disturbances

P. M. Musau[1], B. O. Ojwang[1], M. Kiprotich[1]
[1]Department of Electrical and Information Engineering, University of Nairobi, Nairobi, Kenya
(boazbenson@gmail.com)

Abstract - **This study examines the frequency behaviour of renewable energy power plants after a disturbance (frequency stability) by investigating how renewable energy power plants respond to disturbances in the power system and develop ways to improve frequency stability. The frequency parameters that are investigated include the (Rate of Change of Frequency) ROCOF, nadir frequency, frequency deviation and settling time. Since renewable energy power plants can be fairly discriminated from other plants using their inertia constants, the study of frequency stability can be anchored on the inertia constants. Specifically, the inertia constants of steam, hydro, wind and solar. The study finds that after a disturbance, the power plants get out of sync and causes the same-frequency condition of paralleling generators not to be achieved. It is observed that (Renewable Energy Solution) RES plants with low inertia such as hydro-electric power plants have a higher frequency deviation, high ROCOF, but a lower settling time.**

Keywords - **frequency stability, frequency nadir, inertia constant, rate-of-change-of-frequency**

I. INTRODUCTION

A. Frequency Stability Definition

IEEE/CIGRE joint task force [1] defined frequency stability as the ability of a power system to return to its stable, or normal frequency of operation after a disturbance of different which can arise from extreme loading of the power system, overvoltages, undervoltages, isolation of loads and lines or short-circuit. Based on the nature of the disturbance IEEE/CIGRE also classified power system stability studies into steady state, dynamic and transient stability. Steady state stability analysis involves the analysis of small and gradual changes in the operating conditions of the power system, transient stability involves the analysis of a power system following a large disturbance and, lastly, dynamic stability entails the analysis of small disturbances in the power system [2].

With the insatiable demand for power, more power generating units of different types are being constructed and injected into the national grid. These generating units can broadly be classified as renewable and non-renewable based on the primary source of energy. Renewable sources of energy entails power generation from solar, biomass, wind, biofuels, tidal, hydropower and geothermal while non-renewable sources of energy include nuclear, coal, oil and natural gas [3], [4].

Different power generation sources have unique characteristics and may affect power stability. One of the major characteristics of the power generating units that may affect system stability is whether they plants are synchronous or asynchronous. In synchronous generation, the rotor of the generator is closely coupled to the power system, while in asynchronous power generation like solar power generation, the output frequency is derived from the switching action of the Silicon Controlled Rectifier in the inverter [5]. The idea of rotors and isolation is important in frequency stability of the power system because frequency is a factor of the angular velocity of the rotors. Synchronous generators run at synchronous speed and the synchronous speed is locked to the electrical frequency of the generated voltages and currents, depending on the number of poles of the machine. For synchronous power generation, inertia is an important parameter that provides kinetic energy that will be converted to electrical energy. The motion of the rotor of synchronous machines is founded on the principle that the product of the moment of the inertia and its angular acceleration gives the accelerating torque of the machine. Through this relationship, the swing equation is derived, which is relates the rotor angle, inertia constant, rotor speed and the accelerating power of a synchronous generator [6], [1].

B. Contribution

This study models frequency dynamics using the swing equation and considers the torque damping coefficient to realize a nearly ideal power system behaviour. Scholars agree that one of the main factor that distinguish RES (Renewable Energy Solutions) from other RES and non-RES is the angular mass. The inertia constants of steam, hydro, wind and solar range from 4-9, 2-4, 2-5 and 0 sec, respectively [4].

Furthermore, this study investigates the effect of the angular mass on ROCOF, frequency nadir and settling time. The determination of these relationships is important in predicting power system failures and proactively setting-up primary, secondary, load shedding, synthetic inertia, limited frequency sensitive mode, under or over frequency and tertiary power system protection mechanisms.

II. LITERATURE REVIEW

A lot of research has been done to determine the effect of increased penetration of renewable energy on frequency stability. Using Modal analysis, eigenvalue analysis, participation factors and sensitivity analysis with respect to inertia to demonstrate the influence of the increasing non-synchronous generation based on Full Rated Converters (FRC) on small signal stability, Chamorro, Ghandari and Eriksson [7] identified two dominant modes in their modelled power system and noted that mode shapes movement were oscillatory in the operative areas. From the sensitivity analysis, the authors also observed that the modes are affected by the integration of non-synchronous generation and indicate that it is dependent on the level of penetration. It was also noted that generators with PSS

978-1-5386-7434-5/19/$31.00 ©2019 IEEE

systems were more stable. The authors recommended the addition PSS systems or other control loops to non-synchronous generation. However, the authors failed to relate their findings on voltage stability, rotor angle stability and frequency stability as defined by IEEE/CIGRE joint taskforce.

Musau, Chepkania and Abungu [6] proposed a different approach in enhancing frequency stability. The authors proposed a Combined Frequency with renewable energy Cost (CFS) approach in enhancing frequency stability. In their review of frequency stability, the frequency dynamics elements such as the swing equation and the moment of inertia or angular mass (J) are Equations brought into perspective. The authors used a Scenario Based Method to determine the probabilities of RES in various scenarios generated by the Roulette Wheeling Method. While the authors proposed the CFS approach to frequency stability problems, their study does not clearly address how renewable energy power generation such as wind and solar affects frequency stability elements such as ROCOF and frequency nadir.

Teng and Strbac [8] investigated the benefits of using Synthetic Inertia (SI) and providing (Primary Frequency Response) PFR in wind power plant using multi-stage stochastic scheduling formulation that takes frequency support from wind plants. First, from their results, the authors noted that SI could effectively be used to reduce the system operation cost and the SI provision demand 6 could be significantly reduced by relaxing the ROCOF limit. Secondly, the authors found that with a taut ROCOF limit, providing PFR could provide no value for wind power plants. However, relaxing the ROCOF would make PFR to provide similar cost savings as SI. Lastly, the combination of SI and PFR only achieve marginal benefits as compared to SI only. However, when determining the cumulative SI provision, the study only considers the uncertainty associated with the quantity of wind plants being online. There was a need to develop a more detailed model taking into account the probability distribution of wind ramps and speeds. Additionally, their study fails to model an accurate relationship between the additional PFR requirement and SI provision at equilibrium.

In another study Abdlrahem, Venayagamoorthy and Corzine [5] compared an area with (Photo-Voltaic) PV plants and another area without PV observed that increased PV penetration improved frequency stability by damping out the oscillations caused by a disturbance. The authors used Real-Time Digital Simulator, however, the authors failed to solve for the optimal penetration level of PV to yield optimal but realizable frequency stability. Ciapessoni, Cirio, Gatti and Pitto [9] conducted a similar study by modelling the Sicilian Power System using Italian TSO standards. The authors simulated 30 percent, 50 percent and 100 percent of PV retroffiting and noted that higher retrofitting of PV yielded a higher steady-state frequency, hence, a better frequency security. However, failed to solve for the optimal penetration level of PV to yield optimal but realizable frequency stability.

Sanchez, Soloot and Molinas [10] focused on stability influence of renewable energy systems: connection to DC nanogrids. The authors observed that the Nyquist test with the (Inductor-Capacitor-Inductor) LCL filter was safer compared to the one without the LCL filter because the forbidden region -6dB, 30deg was not 7 crossed. Nevertheless, the authors concluded that the retrofitting RES into the nanogrid did not affect the stability of the system, as long as the safe operation was not exceeded. The authors used the Agilent E5061B network analyzer and hardware-in-the-loop real time simulation (OPAL-RT). They conducted a Nyquist test with the Norton equivalent for the nanogrid and RES with and without an LCL filter. The authors, however, did not clearly define the 'safe operation region'. Additionally, Sanchez et al did not study the behaviour of voltage and frequency after a disturbance.

III. PROBLEM FORMULATION

A disturbance in power angle $\Delta\delta$ from the initial operating point δ_0 is introduced to the swing equation to emulate a physical disturbance in the power system [11]

$$\frac{2H}{\omega}\frac{d^2(\delta_0+\Delta\delta)}{dt^2} = P_m + \Delta P_m - P_{\max}\sin(\delta_0+\Delta\delta) - D\frac{d(\delta_0+\Delta\delta)}{dt} \quad (1)$$

With some approximation, the swing equation with disturbance becomes [11], [12]:

$$\frac{2H}{\omega}\frac{d^2(\delta_0)}{dt^2} + \frac{2H}{\omega}\frac{d^2(\Delta\delta)}{dt^2} = P_m + \Delta P_m - P_{\max}\{\sin(\delta_0) + \cos(\delta_0)\Delta\delta\} - D\frac{d(\delta_0)}{dt} - D\frac{d(\Delta\delta)}{dt} \quad (2)$$

The system under disturbance can be linearized such that the initial state of operation is:

$$\frac{2H}{\omega}\frac{d^2(\delta_0)}{dt^2} = 0 = P_m - P_{\max}\sin(\delta_0) - D\frac{d(\delta_0)}{dt} \quad (3)$$

And the linearized incremental change in power angle Δδ is [11]:

$$\frac{H}{\pi f_0}\frac{d^2(\Delta\delta)}{dt^2} = \Delta P_m - P_S(\Delta\delta) - D\frac{d(\Delta\delta)}{dt} \quad (4)$$

Where $P_S = P_{\max}\cos(\delta_0)$ is the synchronizing power coefficient [11], Equation (4) becomes

$$\frac{d^2(\Delta\delta)}{dt^2} + \frac{\pi f_0}{H}D\frac{d(\Delta\delta)}{dt} + P_S\frac{\pi f_0}{H}(\Delta\delta) = \frac{\pi f_0}{H}\Delta P_m \quad (5)$$

Or in s-domain, we have

$$\Delta\delta = \frac{\pi f_0}{Hs^2}\Delta P_m - \frac{\pi f_0}{Hs}D - P_S\frac{\pi f_0}{Hs^2} \quad (6)$$

Or

$$\dot{\Delta\omega} + \frac{\pi f_0}{H}D\Delta\omega + P_S\frac{\pi f_0}{H}(\Delta\delta) = \Delta P_m \quad (7)$$

$$\dot{\Delta\delta} = \Delta\omega \quad (8)$$

In state-space, we have

$$\begin{bmatrix}\dot{\Delta\omega}\\ \dot{\Delta\delta}\end{bmatrix} = \begin{bmatrix}-\frac{\pi f_0}{H}D & -P_S\frac{\pi f_0}{H}\\ 1 & 0\end{bmatrix}\begin{bmatrix}\Delta\omega\\ \Delta\delta\end{bmatrix} + \begin{bmatrix}\frac{\pi f_0}{H}\\ 0\end{bmatrix}\Delta P_m \quad (9)$$

The state matrix indicates that $(\dot{\Delta\omega})$ ROCOF is dependent on D, H, Ea, Xs and δ_0. Therefore, we can improve ROCOF by optimizing any of these parameters [13].

The disturbed system can also be modelled as a control system with a transfer function:

$$\frac{\Delta\delta}{\Delta P_m} = \frac{\frac{\pi f_0}{H}}{S^2 + S\frac{\pi f_0}{H}D + P_S\frac{\pi f_0}{H}} \quad (10)$$

Which can be modelled as a control system, from equation 6, as shown in Fig. 1.

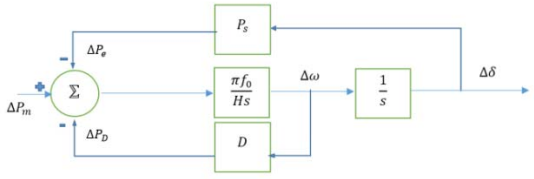

Fig. 1: Block diagram of the disturbed system

The behaviour of the disturbed system is defined by the characteristic equation [12]:

$$S^2 + S\frac{\pi f_0}{H}D + P_S\frac{\pi f_0}{H} = 0 \quad (11)$$

Which takes the standard form of a second order control system [12]:

$$S^2 + 2\zeta\omega_n S + \omega_n^2 = 0 \quad (12)$$

Where the un-damped natural frequency $\omega_n = \sqrt{P_S\frac{\pi f_0}{H}}$, the damping ratio $\zeta = \frac{D}{2}\sqrt{\frac{\pi f_0}{HP_s}}$ and the damped frequency of oscillation $\omega_d = \omega_n\sqrt{1-\zeta^2}$

The settling time is given by [12]:

$$\tau_S = 4\tau \quad (13)$$

Where $\tau = \frac{1}{\zeta\omega_n} = time\ constant$

For a stable and bound system, $0 < \zeta = \frac{D}{2}\sqrt{\frac{\pi f_0}{HP_s}} < 1$ and the transient response of the rotor angle deviation is

$$\Delta\delta(t) = \Delta\delta\frac{e^{-\zeta w_n t}}{\sqrt{1-\zeta^2}}\sin\left\{\omega_d t + \tan^{-1}\left(\frac{\sqrt{1-\zeta^2}}{\zeta}\right)\right\} \quad (14)$$

and the system frequency deviation after the disturbance is defined by

$$\Delta\omega(t) = \Delta\delta\frac{e^{\zeta w_n t}}{\sqrt{1-\zeta^2}}\{-\zeta\omega_n\sin(\omega_d t + \varphi) + \omega_d\cos(\omega_d t + \varphi)\} \quad (15)$$

Where $\varphi = \tan^{-1}(\frac{\sqrt{1-\zeta^2}}{\zeta}) = \cos^{-1}\zeta$

The objective function is modelled as an optimization problem for minimizing frequency deviation after a disturbance as:

$$\min\Delta\omega(t) = min\left\{\Delta\delta\frac{e^{-\zeta w_n t}}{\sqrt{1-\zeta^2}}\{-\zeta\omega_n\sin(\omega_d t + \varphi) + \omega_d\cos(\omega_d t + \varphi)\}\right\} \quad (16)$$

IV. PROPOSED METHOD

A. Optimizing the Damping Coefficients of the System using Firefly Algorithm (FA)

The flashing and behavior of fireflies can be mathematized. The inverse square law provides that as the distance r increases, the intensity of the light I keeps decreasing, that is, $I \propto \frac{1}{r^2}$. For a maximization problem, the brightness I of a flash, at a location x, can be expressed a $I(x) \propto f(x)$. The attractiveness β is relative to the other fireflies and will vary with distance r_{ij} for firefly i and firefly j.

The movement of a firefly i attracted to a brighter (attractive) firefly j is defined by expression:

$$x_i = x_i + \beta_0 e^{-\gamma r_{i,j}^2}(x_i - x_j) + \alpha\left(rand - \frac{1}{2}\right) \quad (17)$$

Where $I_s = \text{brightness of the flash at source}$

$\gamma = \text{forced light absorption coefficient}$

$I_0 = \text{the initial light intensity.}$

$\beta_0 = \text{attractiveness at source,} \quad r = 0$

The second term arises due to the attraction while the third is a randomization with α being a randomized parameter [14]. Optimization of the damping parameter is as follows:

1) Defining grid fed power plants from non-renewable and renewable sources of energy and finding the optimal load flow solution, here, the IEEE 9 bus system is used. From this, the power delivered to the grid and the initial operating point before a disturbance is determined.

2) Given the optimal load flow solution, the synchronizing power P_s coefficient for each power plants and set the system frequency under considerations is then determined from equation, in this case, a system frequency $f_0 = 50Hz$ was used.

3) A disturbance in power angle $\Delta\delta$ from the initial operating point δ_0 is then introduced to emulate a physical disturbance in the power system.

4) Frequency deviation that results from the disturbance is then evaluated. This includes the evaluation of ROCOF, nadir frequency and settling time. In FA, this is the brightest/most attractive firefly at the start of the search for a mating partner.

5) For a specific power plant, defined by a specific inertia constant, the damping of the system is adjusted and the response of the frequency is monitored until the minimum frequency deviation is achieved, as defined by the objective function. The adjustment is done by dispatching n number of fireflies to look for the brightest or the most attractive (minimum frequency deviation) mating partner.

6) The damping coefficient is then updated (the position of the most attractive mating partner up to date). This is iterated until the damping that yields the minimum frequency deviation for a given system inertia constant is found.

TABLE 1
TYPICAL PARAMETER RANGES [6]

Parameter	Value(Range)
Firefly population	15-100
α	[0,1]
γ	0.01-100
$\boldsymbol{\beta_0}$	1
rand	0-1

TABLE 2
PARAMETER MAPPING

Parameter	Mapped Parameter
Firefly population (male and female)	Renewable (male firefly) and non-renewable energy plants (female firefly) in the grid
Randomized parameter (α)	Disturbance in the system caused by power imbalance
Fixed light absorption coefficient (γ)	The angular mass of renewable and non-renewable energy plants
Distance (r)	Amount of renewable energy integrated into the grid with non-renewable energy
Brightness at source ($\boldsymbol{\beta_0}$)	The angular mass of non-renewable energy plants before integrating renewable energy into the grid
Brightness (β)	Damping power of renewable energy systems
Movement ($\boldsymbol{x_i}$)	Movements in system frequency following a disturbance

B. *Using Thyristor Switched Lag Compensator (TSLC) to Improve Frequency Dynamics*

The objective is to improve the system frequency behavior by removing or cutting down overshoots and removing harmonics. This can be achieved by inserting a lag compensator at the function defining the frequency deviation.

Fig. 2 shows the operation of the TSLC in improving frequency dynamics of RES

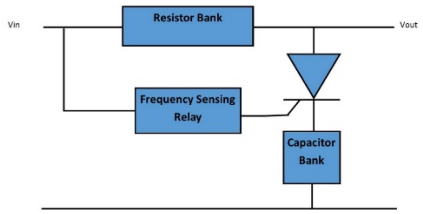

Fig. 2: Thyristor Switched RC Lag Compensator

The transfer function of the compensator is given by:

$$H(s) = \frac{1}{1+sRC} = \frac{1}{1+sk} \quad (18)$$

It can be shown that ROCOF is restrained using TSLC. In state space, the compensator can be represented as:

$$\Delta\omega' = -\frac{1}{k}\Delta\omega + \frac{1}{k} \quad (19)$$

$$y = \Delta\omega \quad (20)$$

The state space representation shows that the system is a first order function with one input and one output. Since the input signal represents the frequency deviation, x oscillates around the grid frequency. As a result, the ROCOF, $\Delta\omega'$, is restrained by setting the value of k

In time domain,

$$h(t) = (1 - e^{-\frac{t}{k}}) \quad (21)$$

The frequency deviation after compensation is therefore a convolution of $h(t)$ and the frequency deviation before compensation, that is,

$$\Delta\omega_{comp}(t) = \Delta\omega(t) * h(t) \quad (22)$$

$$\Delta\omega_{comp}(t) = \left\{\Delta\delta \frac{e^{\zeta w_n t}}{\sqrt{1-\zeta^2}}\{-\zeta\omega_n \sin(\omega_d t + \varphi) + \omega_d \cos(\omega_d t + \varphi)\}\right\} * \left\{1 - e^{-\frac{t}{k}}\right\} \quad (23)$$

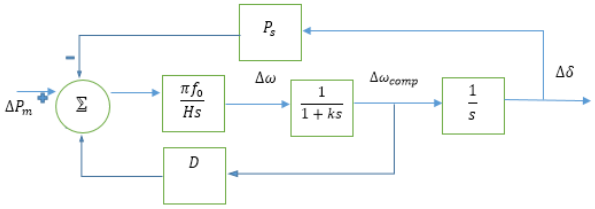

Fig. 3: Block diagram of the disturbed system with TSLC

The proposed bus system for validation is the IEEE 9-bus system consisting of 3 synchronous generators, 6 transmission lines, 3 constant impedance loads, 6 transformers and 12 buses, as shown in Fig. 4.

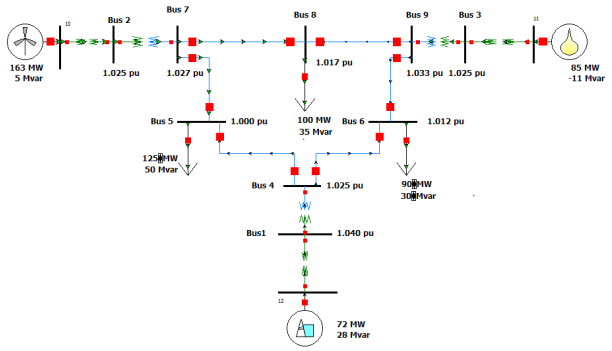

Fig. 4: IEEE 9 Bus System

V. SIMULATED RESULTS

A. *Frequency Stability of RES*

TABLE 3
FREQUENCY DYNAMICS WITH RES BEFORE OPTIMIZATION FOR A 1° POSITIVE CHANGE IN POWER ANGLE

H	RES type	f_nadir (Hz)	t_nadir (sec)	freq_dev (Hz)	ROCOF(Hz/sec)	t_settling (sec)
3	Hydro	49.9772	0.09	-0.0228	-0.2533	0.6366
3.5	Wind	49.9782	0.10	-0.0218	-0.2180	0.7427
6.5	Geo	49.9820	0.14	-0.0180	-0.1286	1.3793

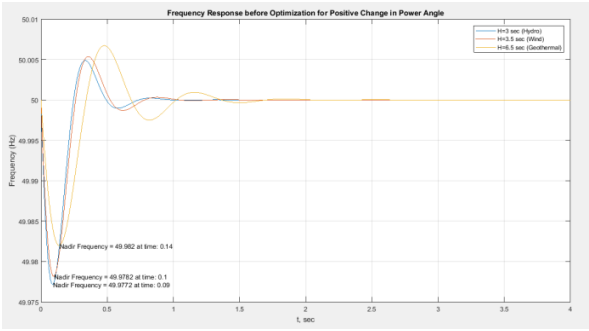

Fig. 5: Frequency Response with RES before Optimization for $+\Delta\delta$

Based on their inertia constants, the results suggest that RES plants have different responses to physical disturbances that cause a change in Power Angle. The frequency deviation negative. For a disturbance that causes a positive change in Power Angle, hydro RES has the highest frequency deviation and ROCOF, but it has the earliest recovery time. It is followed by wind and geothermal RES. Geothermal plants have the least maximum frequency deviation from the nominal frequency by settle later than all the plants. From Table 4, it is observed that a larger change in power angle as a result of a disturbance leads to a larger frequency deviation and ROCOF. However, since this study assumed some linearity in the formulation of the objective function, the accuracy of higher deviations in power angle is not assured. For higher accuracy, the 1° change in power angle is used in this study.

TABLE 4
FREQUENCY DYNAMICS WITH RES BEFORE OPTIMIZATION FOR A 1° NEGATIVE CHANGE IN POWER ANGLE

H	RES Type	f_nadir (Hz)	t_nadir (sec)	freq_dev (Hz)	ROCOF	t_settling (s)
3	Hydro	50.0228	0.09	0.0228	0.2533	0.6366
3.5	Wind	50.0218	0.10	0.0218	0.2180	0.7427
6.5	Geo	50.0180	0.14	0.0180	0.1286	1.3793

For a disturbance that causes a negative change in Power Angle, a similar observation is made as for a

disturbance that causes a positive change in power angle except that the direction of the frequency deviation becomes positive, shown in Table 4.

TABLE 5
FREQUENCY DYNAMICS WITH RES FOR POSITIVE CHANGE IN POWER ANGLE (FA OPTIMIZED)

H	RES Type	f_nadir (Hz)	t_nadir (sec)	freq_dev (Hz)	ROCOF (Hz/sec)	t_settling (sec)
3	Hydro	49.9882	0.06	-0.0118	-0.1967	0.21
3.5	Wind	49.9884	0.07	-0.0116	-0.1657	0.25
6.5	Geo	49.9895	0.11	-0.0105	-0.0955	0.46

TABLE 6
FREQUENCY DYNAMICS WITH RES AFTER OPTIMIZATION FOR POSITIVE CHANGE IN POWER ANGLE (PSO OPTIMIZED)

H	RES Type	f_nadir_Opt (Hz)	t_nadir (sec)	freq_dev (Hz)	ROCOF(Hz/sec)	t_settling (sec)
3	Hydro	49.9878	0.06	-0.0122	-0.2033	0.22
3.5	Wind	49.9881	0.07	-0.0119	-0.1700	0.26
6.5	Geo	49.9892	0.11	-0.0108	-0.0982	0.47

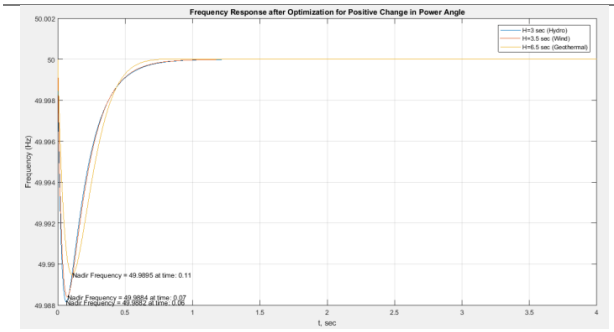

Fig. 6: Frequency Response with RES after FA Optimization for $+\Delta\delta$

TABLE 7
RES FREQUENCY DYNAMICS WITH TSLC FOR $+\Delta\delta$

H (sec)	RES Type	f_nadir (Hz)	freq_dev (Hz)	ROCOF(Hz/sec)	t_settling (sec)
3.0	Hydro	50.0004	0.0004	0.0001	100.0000
3.5	Wind	49.9998	0.0002	0.0000	100.0000
6.5	Geothermal	49.9991	0.0009	0.0002	100.0000

After FA Optimization (Optimal Damping: 0.60577), a decrease in frequency deviation and ROCOF is noted for Hydro, Wind and Geothermal RES. Lastly, the recovery time is improved by 67 percent for all the RES plants. The same is noted for PSO optimization, however, FA optimization was found to have better results.

The TSLC is an effective way to inhibit the frequency deviation. It results in minimal frequency deviations of order $\times 10^{-4} Hz$. A comparison between the unoptimized, FA and PSO optimized and compensated power system, as shown in Fig. 8, indicates that Particle Swarm Optimization (PSO) optimized system has a better nadir frequency than the unoptimized system, while FA optimized system offers a better nadir frequency than PSO optimized system and the compensated system has the best nadir frequency for the renewable energy power plants considered (Hydro, Wind and Geothermal).

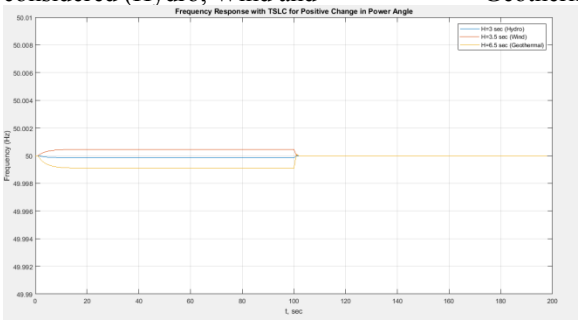

Fig. 7: RES Frequency Response with TSLC for -Δδ

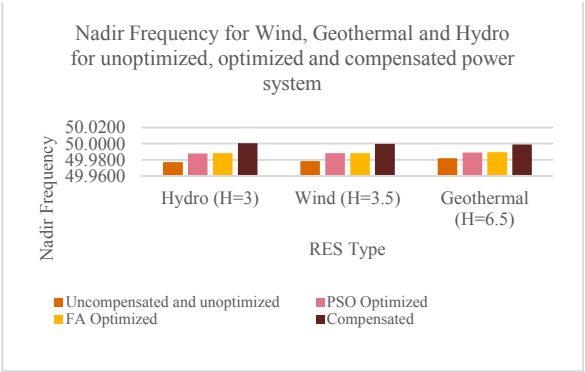

Fig. 8: Nadir Frequency for Wind, geothermal and hydro for unoptimized, optimized and compensated power system

B. *Kenyan Case Study*

The formulated model was used to study the frequency behaviour of Kenyan power plants based on their inertia constants (H), obtained from Kenya Electricity Generating Company (KenGen) [15]. The results are as shown in Fig. 9.

From Fig. 9, it is observed that Rabai Power Plant Generator 6, a thermal power plant, has the lowest nadir frequency (furthest to the nominal frequency of 50Hz). Mumias G1, G2 and G3, which are Biomass (bagasse) Power Plants, are seen to have the second lowest nadir frequency of 49.972Hz. Kwale Sugar and Muhoroni Sugar, also Bagasse Power Plants, show a relatively low nadir frequency of 49.9749Hz. This is attributed to their low inertia.

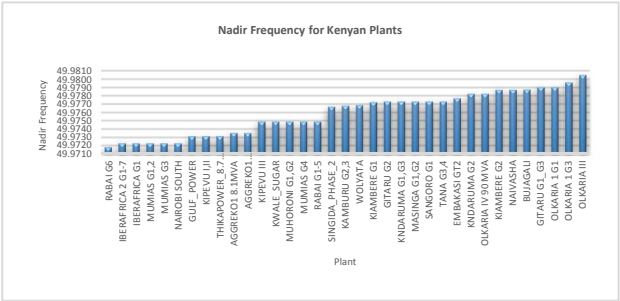

Fig. 9: Nadir Frequencies for Kenyan Power Plants

Olkaria III has the highest nadir frequency of 49.9805Hz (closest to the nominal frequency of 50Hz). Being a Geothermal power plant Olkaria III has a higher inertia constant, this explains why it has a closer frequency to the nominal frequency. Olkaria I G1-G3, also Geothermal Power Plants, exhibit the second highest nadir frequency of approximately 49.98Hz. Gitaru G1-G3, Bujagali, Kiambere G2 and Kindaruma G2, hydroelectric power plants, exhibit a higher nadir frequency than Biomass Power Plants (Mumias G1, G2, G3, Kwale Sugar and Muhoroni Sugar), but lower than Geothermal Power Plants (Olkaria I and III).

VI. CONCLUSION

Since different renewable energy power plants have different inertia constants, this study finds that it is possible to determine the frequency behavior of renewable energy power plants including wind, hydro and geothermal power plants after a disturbance. This study finds that a

disturbance that causes a positive change in power angle will lead to underfrequency while a negative change in power angle will lead to overfrequency. From the simulation using IEEE 9 Bus System Parameters, it was observed that the hydro-electric power plant, wind power plant and geothermal power plant have a maximum frequency deviation of 0.0228Hz, 0.0218Hz and 0.0180Hz respectively as a result of a disturbance that causes a 1-degree change in power angle, indicating that the geothermals are more stable, followed by wind plants and hydros, respectively.

The study of Kenya's renewable power plants finds that Biomass (bagasse) such as Mumias Sugar Power Plant, Kwale Sugar and Muhoroni Sugar Power Plants and have the largest maximum frequency deviation in case of a 1° disturbance, causing a nadir frequency of 49.9723Hz-49.9749Hz. Hydro-electric power plants including Gitaru G1-G3, Bujagali, Kiambere G2 and Kindaruma G2 have a lower frequency deviation, which results to a nadir frequency of approximately 49.9773Hz. Lastly, the results suggest that geothermal power plants have the lowest frequency deviation leading to a nadir frequency of 49.9805Hz. It is also observed that larger changes in power angle causes larger frequency deviations. A 20° change in power angle was tested and found to yield frequency deviations of 0.3607Hz, 0.4368Hz and 0.4569Hz for hydro, wind and geothermal power plants respectively.

VII. RECOMMENDATIONS

Future studies may consider frequency dynamics of power plants where $\zeta^2 > 1$ or $\zeta^2 = 1$. Secondly, future studies may investigate transient stability with RES. Future studies may also address non-synchronous renewable power plants such as solar and converter based wind power plants. The frequency dynamics of these converter based power plants is a power electronics problem. Other optimization techniques such as ACO, GA and BA may be used and the results compared with the findings of this study. Larger IEEE bus systems may be also used.

VIII. REFERENCES

[1] P. Kundur, J. Paserba, V. Ajjarapu, G. Andersson and B. Canizares, "Definition and Classification of Power System Stability," *IEEE Transactions on Power Systems,* vol. 19, no. 2, 2004.

[2] M. J. Basler and C. Schaefer, "Understanding Power-System Stability," *IEEE Transactions on Industry Applications,* vol. 44, no. 2, 2008.

[3] D. A. Woldeyohannes, D. E. Woldemichael and T. A. Baheta, "Sustainable renewable energy resources utilization in rural areas," *Renewable and Sustainable Energy Reviews,* vol. 66, no. 1, pp. 1-9, 2016.

[4] J. O'Sullivan, A. Rogers, D. Flynn, P. Smith, A. Mullane and M. O'Malley, "Studying the Maximum Instantaneous Non-Synchronous Generation in an Island System—Frequency Stability Challenges in Ireland," *IEEE Transactions Power Systems,* vol. 29, no. 6.

[5] A. Abdlrahem, G. K. Venayagamoorthy and K. A. Corzine, "Frequency Stability and Control of a Power System with Large PV Plants Using PMU Information," *North American Power Symposium (NAPS),* 2013.

[6] P. M. Musau, T. L. Chepkania, A. N. Abungu and C. W. Wekesa, "Effects of Renewable Energy on Frequency Stability: A Proposed Case Study of the Kenyan Grid," *IEEE PES-IAS PowerAfrica,* 2017.

[7] H. Chamorro, M. Ghandhari and R. Eriksson, "nfluence of the Increasing Non-Synchronous Generation in Small Signal Stability," *PES General Meeting | Conference & Exposition IEEE,* 2014.

[8] F. Teng and G. Strbac, "Assessment of the Role and Value of Frequency Response Support from Wind Plants," *IEEE Transactions on Sustainable Energy,* 2016.

[9] E. C. D. G. A. Ciapessoni and A. Pitto, "Renewable power integration in Sicily: Frequency stability issues and possible countermeasures," *Bulk Power System Dynamics and Control - IX Optimization, Security and Control of the Emerging Power Grid (IREP), IEEE,* 2013.

[10] S. S. H. A. Sanchez and M. Molinas, "Stability influence of renewable energy systems: connection to DC nanogrids," *Control and Modeling for Power Electronics (COMPEL) 17th Workshop,* 2016.

[11] J. J. Grainger and w. d. Stevenson, "Power System Stability," in *Power System Analysis*, McGrawHill, 1994.

[12] K. Ogata, Modern Control Engineering, Pearson Education International, 2002.

[13] M. El-Shimy, "Dynamic Security of Interconnected Electric Power Systems," *LAP,* vol. 2, 2015.

[14] X. S. Yang, Firefly Algorithms for Multimodal Optimization, University of Cambridge – Department of Engineering, 2009.

[15] J. Sutter and P. Mburu, "Power System Stability Improvement with Geothermal as a Major Source of Power in Kenya," *Proceedings, 6th African Rift Geothermal Conference,* 2016.

[16] A. K. Kumar, M. P. Selvan and K. Rajapandiya, "Grid stability analysis for high penetration solar photovoltaics," *1st International Conference on Large-Scale Grid Integration of Renewable Energy in India,* 2017.

[17] K. Maslo, "Impact of Photovoltaics on Frequency Stability of Power System During Solar Eclipse," *IEEE Transactions on Power Systems,* vol. 31, no. 5, 2016.

[18] European Network of Transmission System Operators for Electricity (ENSOE), "Frequency Stability Evaluation Criteria for the Synchronous Zone of Continental Europe," 2016.